16 Determination of Parastichy Numbers and Its Applications

Riichirou Negishi

CONTENTS

16.1 Introduction 241
16.2 Simulation Models 244
16.2.1 Sunflower Model (S-Model) 244
16.2.2 Pineapple Model (P-Model) 245
16.3 Analysis Procedure Using a Discrete Fourier Transform 247
16.3.1 The Sunflower Model 247
16.3.2 The Pineapple Model 248
16.4 Analytical Results 248
16.4.1 Parastichy Numbers Near the Golden Angle in Sunflower Models 248
16.4.2 Parastichy Numbers for Wide Divergence Angles in Sunflower Models 252
16.4.3 Parastichy Numbers in Pineapple Models 253
16.5 Discussion 255
16.5.1 Difference in the Numbers of Sample Points 255
16.5.2 Difference in Index p 256
16.5.3 Sampling Position 257
16.6 Applications 257
16.6.1 A Part Sampling 257
16.6.2 Evaluation of Disturbance 258
16.6.3 Applying to a Real Sunflower 260
16.7 Summary 261
References 261

16.1 INTRODUCTION

Sunflower florets or seeds are arranged in spirals on the head inflorescence. Spiral arrangements are characterized by the number of curves winding clockwise (CW) and counterclockwise (CCW), and the number of curves forming spirals is called parastichy number. The parastichy numbers often demonstrates the Fibonacci number. Also, the ratio of CW/CCW or CCW/CW in the spiral arrangement is

K377360_C016.indd 241 01/12/19 8:34:16 PM

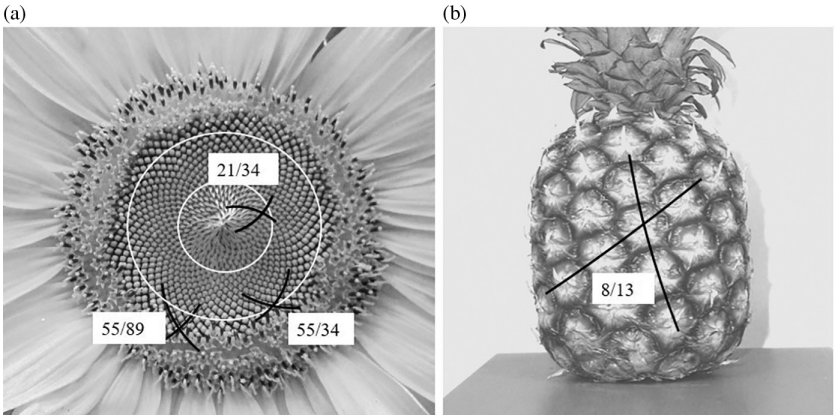

FIGURE 16.1 (a) the pattern of seeds on a sunflower head; and (b) ramenta on a pineapple, displaying as Fibonacci numbers. Each number is counted along black lines.

approximately equal. In the eighteenth century, Johannes Kepler observed that Fibonacci numbers were common in plants (Adler et al., 1997). When we visually count the spirals toward the outer region on a sunflower head, we find 21/34, 34/55, and 55/89 (CW or CCW) as the parastichy numbers (Figure 16.1a). Furthermore, when we visually count the helical numbers along the black line on pineapple skin, we find 8 and 13 corresponding to Fibonacci numbers (1, 1, 2, 3, 5, 8, 13, 21, 34, 55, 89,…) (Figure 16.1b). These parastichy numbers have attracted much attention from researchers for centuries (Vogel, 1979).

Sunflower seed spirals have been studied by a number of scientists following Hofmeister's (1868) systematic description of the phyllotaxis mechanism including spiral formation (Adler et al., 1997; Mathai and Davis, 1974). Alan Turing sketched seed patterns and studied Fibonacci phyllotaxis (Turing, 1952, 1956). Van der Linden (1990) obtained a sunflower spiral-like formation via the dislodgement model without using divergence angles. Dunlap (1997) emphasized the fundamental properties of Fibonacci numbers and their application to diverse fields including mathematics, computer science, physics, and biology. Negishi and Sekiguchi (2007) has proposed an application that offered the possibility of transmitting information at high speed or prohibiting the moiré fringe in image processings.

Such spirals and parastichy numbers have also drawn attention in various model systems including laboratory experiments. For example, Douady and Couder (1992) successfully obtained Fibonacci spirals with drops of ferrofluid under the influence of a magnetic field. Spiral structures are emerging as powerful nanophotonic platforms with distinctive optical properties for multiple engineering applications (Agrawal et al., 2008; Trevino et al., 2008; Liew et al., 2011; Negro et al., 2012).

Adler (1974) proposed a theorem to determine the number sequences for various divergence angles. Jean (2009) summarized the relationship between the divergence angles and the number sequences using Adler's theorem. Table 16.1 shows the calculated number sequences for various divergence angles using Adler's theorem. In Table 16.1, the Fibonacci sequence is denoted by F, the Lucas sequence is denoted

TABLE 16.1
Number Sequences for Various Divergence Angles

Divergence Angle	Sequences
137.51°	*F,G*(1,2): 1, 2, 3, 5, 8, 13, 21, 34, 55, 89, 144, 233, 377, 610, 987, 1597,…
99.50°	*L,G*(1,3): 1, 3, 4, 7, 11, 18, 29, 47, 76, 123, 199, 322, 521, 843, 1364,…
77.96°	*G*(1,4): 1, 4, 5, 9, 14, 23, 37, 60, 97, 157, 254, 411, 665, 1076, 1741,…
64.08°	*G*(1,5): 1, 5, 6, 11, 17, 28, 45, 73, 118, 191, 309, 500, 809, 1309, 2118, …
54.40°	*G*(1,6): 1, 6, 7, 13, 20, 33, 53, 86, 139, 225, 364, 589, 953, 1542, 2495, …
47.25°	*G*(1,7): 1, 7, 8, 15, 23, 38, 61, 99, 160, 259, 419, 678, 1097, 1775, 2872, …
151.14°	*G*(2,5): 2, 5, 7, 12, 19, 31, 50, 81, 131, 212, 343, 555, 898, 1453, 2351, …
158.15°	*G*(2,7): 2, 7, 9, 16, 25, 41, 66, 107, 173, 280, 453, 733, 1186, 1919, 3105, …
162.42°	*G*(2,9): 2, 9, 11, 20, 31, 51, 82, 133, 215, 348, 563, 911, 1478, 2385, 3863, …
68.75°	2 *G*(1,2): 2, 4, 6, 10, 16, 26, 42, 68, 110, 178, 288, 466, 754, 1220, 1974, ...

by *L*, and the generalized Fibonacci sequences are denoted by *G* (Koshy, 2001). Two successive numbers can be expressed as follows:

$$\lim_{n\to\infty} \frac{G_{n+1}}{G_n} = 1.61803... \to \tau \tag{16.1}$$

For a divergence angle of 137.51°, which is approximately equal to the golden angle (137.507764…°), the parastichy numbers demonstrate the Fibonacci sequence (*F*). When the divergence angle is 99.50°, the parastichy numbers give the Lucas sequence (*L*). Generalized Fibonacci sequences (*G*) appear for specific divergence angles, such as 77.96°, 64.08°, and so forth. The point distribution in this simulation fills the plane mostly uniformly.

Even spirals with significantly different structures can be obtained by making a slight difference in divergence angles. For example, in the sunflower model simulation, when a divergence angle is slightly smaller (137.4°) than the golden angle (Figure 16.2a in Section 16.2.1), the parastichy numbers at the outer region consist of the Fibonacci number (*F*) 55 and the Lucas number (*L*) 76. In addition, when the divergence angle is 137.45°, the parastichy number at the outer region only consists of *F* 55 (Figure 16.2b), and when the divergence angle is 137.8°, the parastichy numbers at the outer region are *L* 47 and 81 in *G* (2, 5), consisting all of *F, L*, and *G* sequences (Figure 16.2c). In these cases, the parastichy numbers cannot be calculated using Adler's theorem. Since novel Fibonacci and non-Fibonacci structures in sunflowers have recently been reported (Swinton et al., 2016), we need a practical method to systematically compute parastichy numbers of any spiral patterns.

Vogel (1979) was one of the first researchers to develop a mathematical spiral model to approximate the complex arrangements of florets on a sunflower head. However, Vogel's spirals lack both translational and orientational symmetry in reality. Accordingly, the Fourier space of Vogel's spirals do not exhibit well-defined Fourier peaks, though they show diffuse circular rings, similar to the electron diffraction patterns observed in amorphous solids and liquids (Trevino et al., 2008).

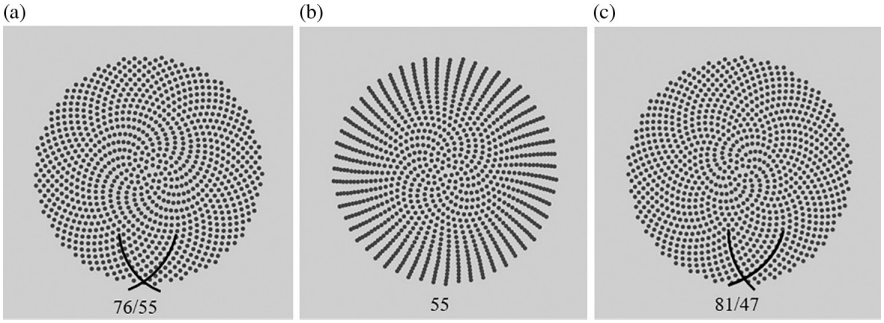

FIGURE 16.2 Simulated point pattern of a sunflower model with a divergence angle of: (a) 137.4°; (b) 137.45°; and (c) 137.8° at $n = 1000$.

This suggests that point distances in a short range are required to analyze spirals. Liew et al. (2011) applied the Fourier–Bessel transform to understand the structural complexity of the golden angle spiral. Negishi et al. (2017) has showed that the parastichy number can be directly measured using the discrete Fourier transform. Fourier transforms are widely used to grasp the characteristics of periodic and aperiodic patterns in natural phenomena and to analyze crystal structures via X-ray diffraction (Authier, 2001; Kikuta, 2011).

Through this chapter, applicability of the proposed method is tested with sunflower and pineapple models. The discrete Fourier transform is applied to the simulated point patterns, and their parastichy numbers with various divergence angles are carefully analyzed.

16.2 SIMULATION MODELS

In this study, two simulation models are used. One is called a sunflower model when the filling points form a circle; the other model is called a pineapple model when the filling points form a rectangle (Negishi et al., 2017).

16.2.1 Sunflower Model (S-Model)

For a sunflower model, the point positions can be determined by the following equation in polar coordinates (Figure 16.3):

$$\left(r,\theta\right)=\left(n^{p},n\varnothing\right) \tag{16.2}$$

Here, n is an integer, p is a constant scaling factor, and ϕ is the divergence angle. When $n = 1000$, p = constant, and $\varnothing = \varnothing_{\tau}$, the points form the spiral shape (Figure 16.4). When $p = 0.2$, dominant parastichy numbers can be visually counted as 55/89 in the outer region (Figure 16.4a). When $p = 0.5$, dominant parastichy numbers can be counted as 21/34, 34/55, and 55/89 in the inner, middle, and outer regions, respectively (Figure 16.4b). And when $p = 1.0$, the numbers in the outer region is 34/55

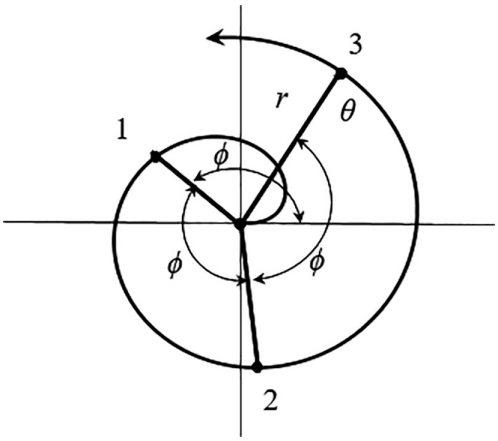

FIGURE 16.3 Spiral trajectory of a sunflower model.

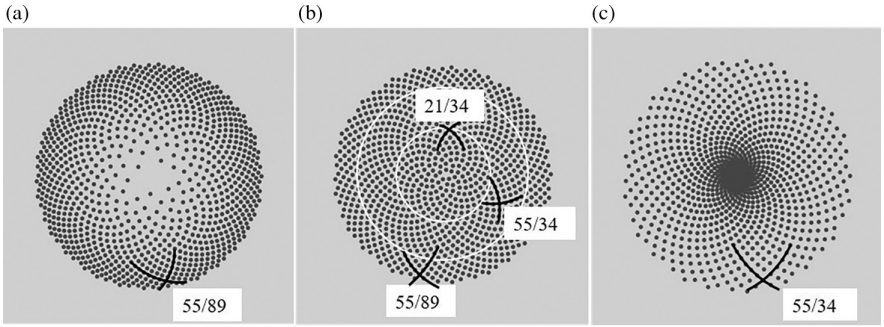

FIGURE 16.4 Simulated point pattern of a sunflower model with n = 1000, p = 0.5, and $\phi = \phi_\tau$. Each number is counted along black lines: (a) p = 0.2; (b) 0.5; and (c) 1.0.

(Figure 16.4c). These numbers correspond to Fibonacci numbers. The parastichy numbers vary depending on the values of n, p, and ϕ, as described later. In the following discussion, $p = 0.5$ is selected because the points can be uniform in the plane. In order to know parastichy numbers by varying p, we will discuss in Section 16.5.

16.2.2 Pineapple Model (P-Model)

A pineapple model is expressed by points on the surface of a cylinder (Figure 16.5). The height l and the argument angle θ are determined by n, p, and ϕ. Point positions on the cylinder for a pineapple model can be generated as follows: $(l, \theta) = (n^p, n\varnothing)$ Figure 16.5 shows point positions with n = 20, p = 1, and $\varnothing = \varnothing_\tau$.The points are patterned after the cylinder being vertically sliced open when n = 1000 and $\varnothing = \varnothing_\tau$. Figure 16.6a–c correspond to p = 0.5, 1, and 2, respectively. When p = 1, the points fill a rectangle having a horizontal side of 2π and a vertical side of l. The points

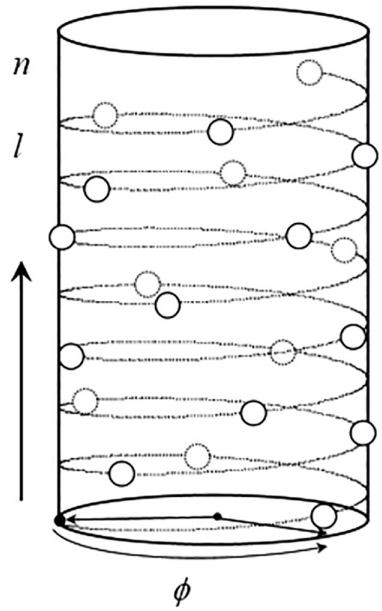

FIGURE 16.5 A pineapple model expressed by points on the surface of the cylinder.

form a series of straight lines (Figure 16.6b). The parastichy numbers around the top of the cylinder are visually counted as 13, 21, 34, and 55, which correspond to Fibonacci numbers (F). When $p = 0.5$ and $p = 2.0$, the points form a series of curves (Figure 16.6a and c). In the following discussion, $p = 1.0$ is selected because of a straight line that the points form. We will discuss parastichy numbers by varying p in Section 16.5.

AQ 1

The parastichy numbers of pineapple models also vary depending on the values of n, p, and ϕ.

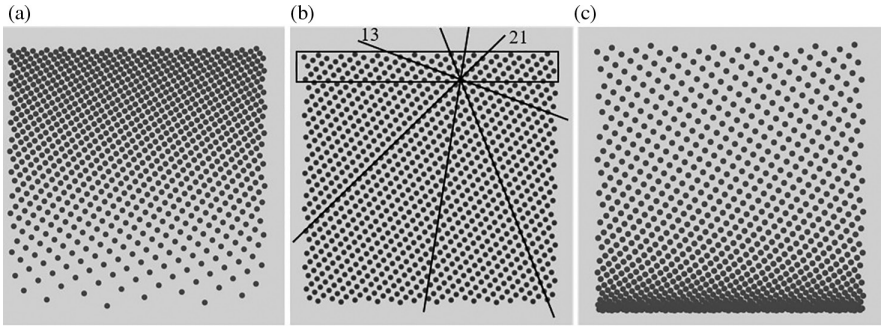

FIGURE 16.6 Simulated point pattern of a pineapple model with $n = 1000$, $p = 1$, and $\phi = \phi_\tau$. The black rectangle shows a measured area to find the parastichy numbers: (a) is $p = 0.5$; (b) 1.0; and (c) 2.0.

16.3 ANALYSIS PROCEDURE USING A DISCRETE FOURIER TRANSFORM

16.3.1 The Sunflower Model

In this section, we propose a method in which discrete Fourier transform is used to compute parastichy numbers in sunflower models. We focus on a short-range arrangement of the seeds (points) at a given radius since the overall arrangement of seeds on the sunflower head (the parastichy number) is a variable spiral structure. Figure 16.7a shows the simulated point pattern in the outer region of the pattern in (Figure 16.4b) when $n = 1000$, $p = 0.5$, and $\varnothing = \varnothing_\tau$. Our method is based on a discrete Fourier transform analyzing a set of distances from each point to its closest point in the spiral pattern. A Fourier transform peak position (spatial frequency) corresponds to a parastichy number. The number of sample points for the discrete Fourier transform is selected to be a power of 2, that is, 256 points in Figure 16.7a. First, an azimuth angle θ for each point is calculated, and the sample data is arranged in ascending order of their angles. Then, the distance from each point to its closest point with a larger angle is measured, and a dataset is created. Figure 16.7b shows the state from the first to the fifth closest point measured from their reference points. Using the Wolfram mathematical software package, a one-dimensional discrete Fourier transform is applied to the dataset. Figure 16.8 shows the absolute value of the Fourier transform spectra. Due to conjugate symmetry for real sequences, the half of the data range is shown. The same procedure is carried out to the second, third, fourth, and fifth closest points. Finally, the Fourier data is summed from the first closest to the fifth closest points to obtain a more accurate power spectrum. As a result, we found that the sum up to the fourth closest point reflects the accurate results. For that reason, hereafter we will analyze parastichies using the sum from the first to the fourth (Figure 16.9).

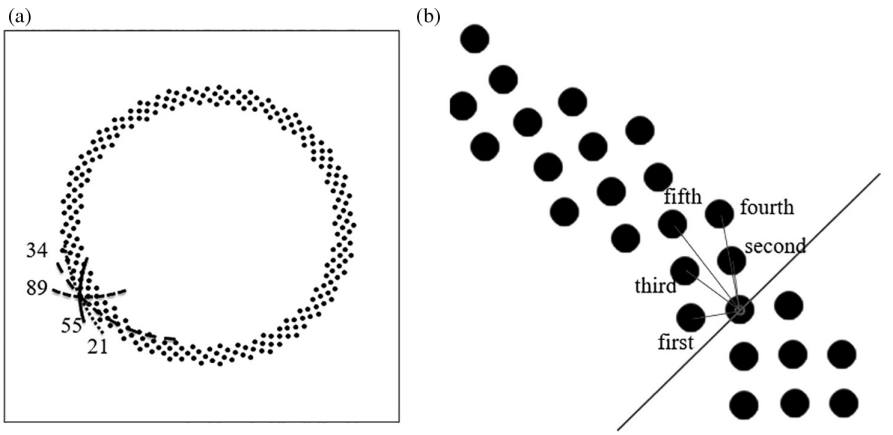

FIGURE 16.7 (a) simulated point pattern in the outer region of a sunflower model with $n = 1000$, $p = 0.5$, and $\phi = \phi_\tau$, showing parastichy numbers of 21/34, 34/55, and 55/89; and (b) closest points for target points.

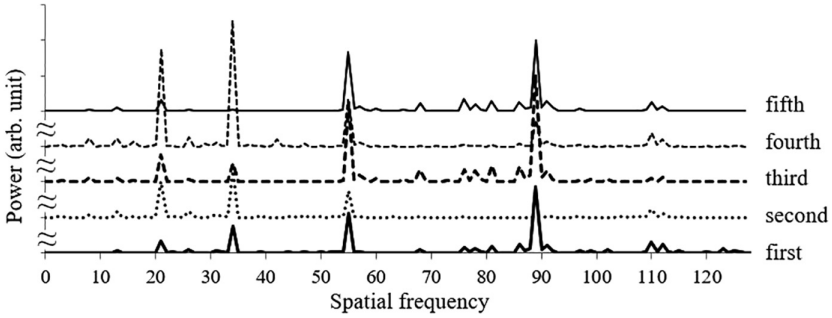

FIGURE 16.8 One-dimensional discrete Fourier transform results for the first, second, third, fourth, and fifth closest points in a sunflower model with $n = 1000$, $p = 0.5$, $\phi = \phi_\tau$, and 256 sample points.

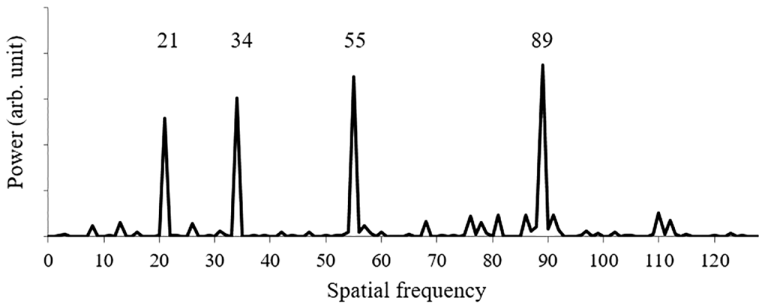

FIGURE 16.9 The Fourier transform result (sum of the data from the first closest points to the fourth closest points in Figure 16.8).

In Figure 16.9, four large peaks can be observed with spatial frequencies of 21, 34, 55, and 89. These values agree with the parastichy numbers visually counted in Figure 16.7. This indicates that parastichy numbers can be determined using the Fourier transform method presented.

16.3.2 The Pineapple Model

We used the same method to determine parastichy numbers in a pineapple model. The number of sample points is 256 points in the black rectangle (Figure 16.6).

16.4 ANALYTICAL RESULTS

16.4.1 Parastichy Numbers Near the Golden Angle in Sunflower Models

This section compares the parastichy numbers determined at the golden angle $\varnothing_\tau$ (the Sunflower model in Section 16.3.1) with those determined at near the golden angle, $\varnothing_\tau$ for the sunflower model. The numbers are both computed using the Fourier transform method. When a point pattern is simulated with $\phi = 137.45°$, which is

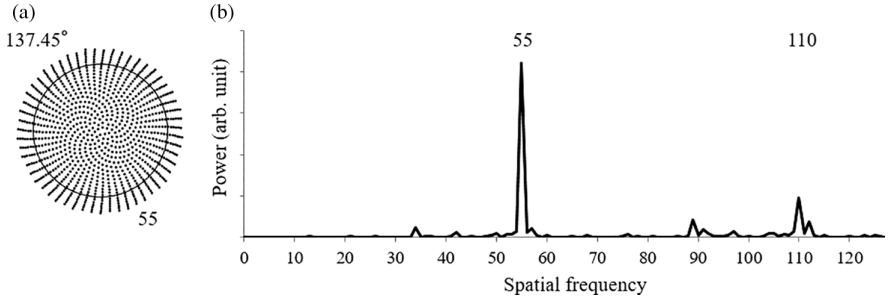

FIGURE 16.10 (a) simulated point pattern for a sunflower model with $\phi = 137.45°$ and $n = 1000$; and (b) Fourier transform result for the area outside the black circle in panel (a).

slightly smaller than $\varnothing_\tau$ interestingly, the points radiated outward in all directions (Figure 16.10a). The Fourier transform results from the outer region showing two large peaks at 55 and 110 (Figure 16.10b). The number 55 is a Fibonacci number, and the number 110 should be the second harmonic wave of 55. Harmonic waves seem to appear as a characteristic feature of the Fourier transform. Figure 16.11a is the simulated point pattern for the case of $\phi = 137.55°$, which is slightly greater than $\varnothing_\tau$. The Fourier transform result from the outer region show the large peaks at 34 and 89 (Figure 16.11b). These numbers agree with those counted visually in the point pattern of Figure 16.11a and are Fibonacci numbers.

When the angles are changed from 137.25° to 137.75° in increments of 0.05° when $n = 1000$ and $p = 0.5$, the Fourier transform results show Fourier peaks at 21, 55, and 76 for a divergence angle of 137.35°. The parastichy numbers 21 and 55 are Fibonacci numbers, while the number 76 is a Lucas number. In addition, the spatial frequency of 97 is observed at a divergence angle of 137.30°. The number 97 belongs to the generalized Fibonacci sequence $G(1, 4)$ according to Table 16.1. Even with a slight change in the angles, like 137.25° to 137.75°, the parastichy numbers can be accurately counted and classified via the presented Fourier transform method (Figure 16.12).

How about when the divergence angle is near 99.50°? Figure 16.13 shows the Fourier results when the angles are changed from 99.25° to 99.75° in increments of 0.05° with $n = 1000$ and $p = 0.5$. When the divergence angles are 99.45° and 99.50°,

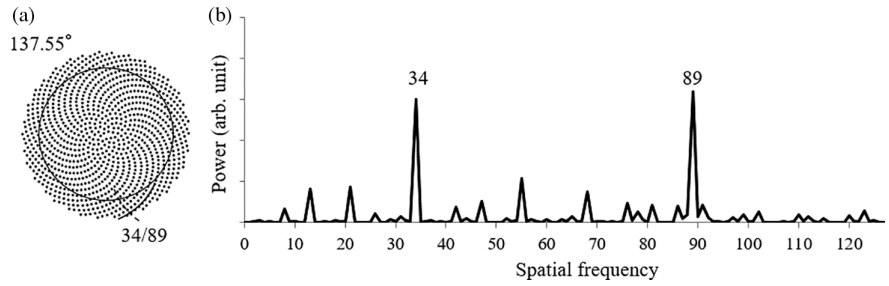

FIGURE 16.11 (a) simulated point pattern for a sunflower model with $\phi = 137.55°$ and $n = 1000$; and (b) Fourier transform result for the area outside the black circle in panel (a).

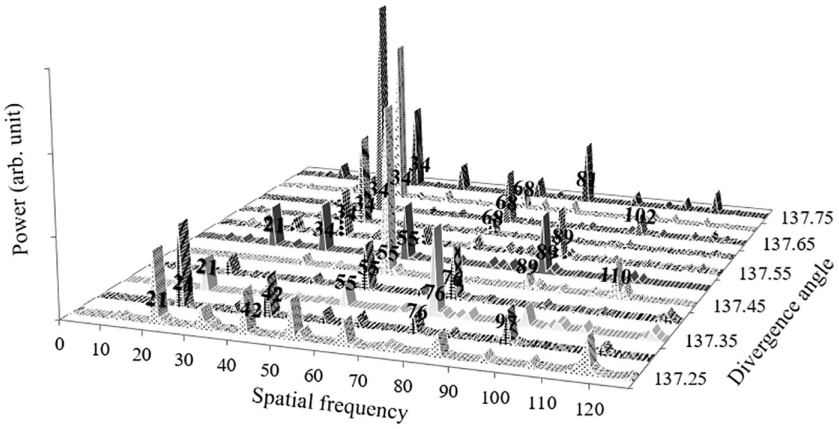

FIGURE 16.12 Fourier transform results near the golden angle ϕ_τ in sunflower models with $n = 1000$ showing various parastichy numbers.

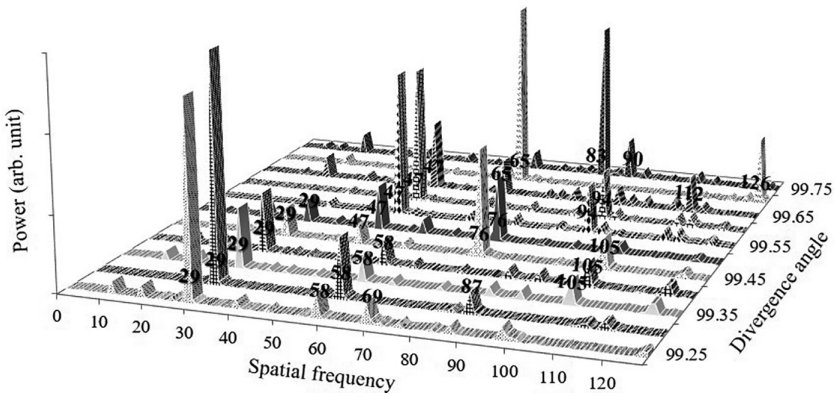

FIGURE 16.13 Fourier transform results near the divergence angle $\phi = 99.50°$ in sunflower models with $n = 1000$ showing various parastichy numbers.

Fourier peaks 29, 47, and 76 are noted as Lucas numbers. At 99.55° and 99.60°, the maximum peak shifts to 47, and the harmonic wave, 94, also increases. When the divergence angle reaches 99.65°, the peak 65 (= 13 × 5) appears, and when the angle is 99.70°, the peak becomes extremely strong. And a large peak 83 appears at 99.75°. On the other hand, the frequency 29 becomes strong at 99.35° and 99.40°, and the second harmonic wave 58 also appears. Furthermore, when divergence angles are 99.25° and 99.30°, the peak 29 is extremely strengthened and the harmonic wave 58 is enlarged. The parastichy numbers resulted from angle changes around 99.50° are centered on the Lucas sequence.

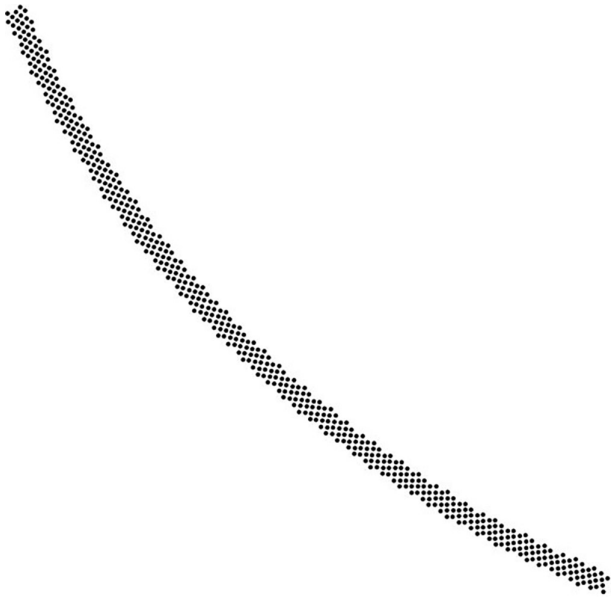

FIGURE 16.14 One part of the simulated point pattern in the outer region of a sunflower model with $p = 0.5$ and $\phi = \phi_\tau$.

When parastichy numbers are visually counted from point patterns, points are highly likely to be miscounted due to extremely dense points (Figure 16.14). The Fourier transform method is used to assess its effectiveness to determine the parastichy numbers with dense points. The number of sampled points for the Fourier transform is 4096 in the outer region. Large Fourier peaks are observed at 610, 987, and 1597, corresponding to Fibonacci numbers (Figure 16.15). This result shows that the parastichy numbers with even a large point pattern can be accurately computed using the proposed method. Lucas numbers, 843 and 1364, though they were relatively small, are also included.

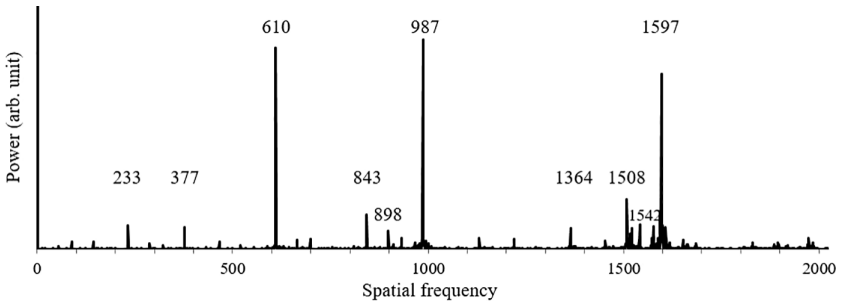

FIGURE 16.15 Fourier transform result for $n = 100000$, $p = 0.5$, and $\phi = \phi_\tau$.

16.4.2 Parastichy Numbers for Wide Divergence Angles in Sunflower Models

This section discusses the effectiveness of the proposed determining method for various divergence angles. The results are summarized in Table 16.1. The point patterns are simulated using the sunflower model with divergence angles of 47.25°, 54.40°, 64.08°, 77.96°, 99.50°, 151.14°, 158.15°, and 162.42°. The parastichy numbers are computed using the discrete Fourier transform (Figure 16.16). All the results agree with those in Table 16.1. When the divergence angle is 47.25°, large Fourier peaks appear at 38 and 61. These numbers belong to G (1,7). For 54.40°, Fourier peaks appear at 20, 33, and 53. These numbers are included in G (1,6). For 64.08°, Fourier peaks 17, 28, and 45 are included in G (1,5); peaks 37 and 60 for 77.96° are included in G (1,4); and peaks 11, 18, 29, and 47 for 99.50° belong to Lucas sequences, that is, G (1,3). Furthermore, peaks (31, 50) for 151.14° belong to G (2,5); (25, 41) for 158.15° belong to G (2,7); and (31, 51) for 162.42° belong to G (2,9). All peaks numbers agree with the results in Table 16.1.

In addition, we examine the parastichy numbers for a divergence angle, 99.65°. It is slightly larger than a divergence angle, 99.50° as we have shown in Figure 16.13. Even though the angle difference between them is only 0.15°, the parastichy numbers cannot be inferred from Adler's theorem. The simulated point pattern and the results by the Fourier transform are shown in Figure 16.17a. The visually counted parastichy numbers are 47, 65, and 112. The Fourier transform results demonstrate the same numbers (Figure 16.17b). This indicates that the proposed Fourier method is highly effective to elucidate a complex structure of generalized Fibonacci sequence with arbitrary divergence angle.

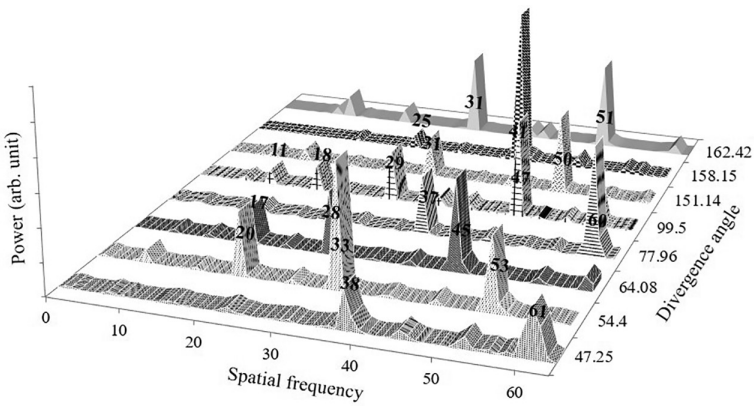

FIGURE 16.16 Fourier transform results showing various spatial frequency (parastichy numbers) when the divergence angles are 47.25°, 54.40°, 64.08°, 77.96°, 99.50°, 151.14°, 158.15°, and 162.42°.

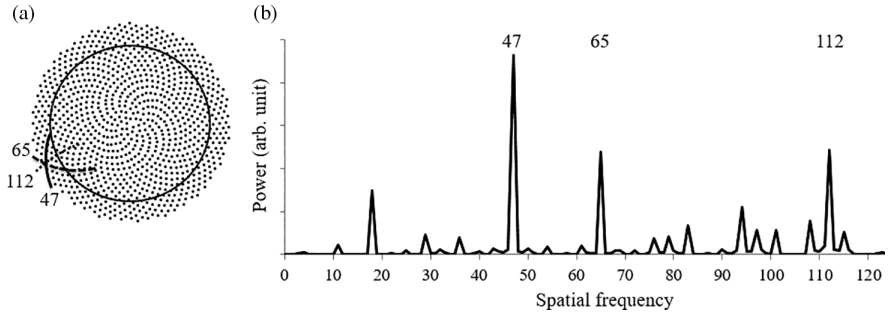

FIGURE 16.17 (a) simulated point pattern; and (b) Fourier transform result for a divergence angle, 99.65° for the region outside the black circle in panel (a).

16.4.3 Parastichy Numbers in Pineapple Models

In this section, the parastichy number of the pineapple model (see pineapple model in Section 16.2.2) is investigated using the presented Fourier transform method. Point patterns of a pineapple model when $n = 1000$ and $p = 1$ is simulated by making changes in the divergence angles. Figure 16.18a and b show the point pattern with $\phi = \phi_\tau$ and its Fourier transform result, respectively. Sample numbers are 128 points. Large Fourier peaks at 13, 21, 34, and 55 are observed, corresponding to the Fibonacci sequence (see also Figure 16.6). Thus, the proposed method is also effective in finding parastichy numbers on the plane as seen in the pineapple model. When $\phi = 137.8°$, some nonuniformity for the distribution is observed (Figure 16.19a). The Fourier peaks of 13, 34, and 47 are observed (Figure 16.19b), and they agree with the parastichy numbers visually counted (panel a). Because the number 47 is a Lucas number, the parastichy numbers are a combination of Fibonacci and Lucas numbers in this case.

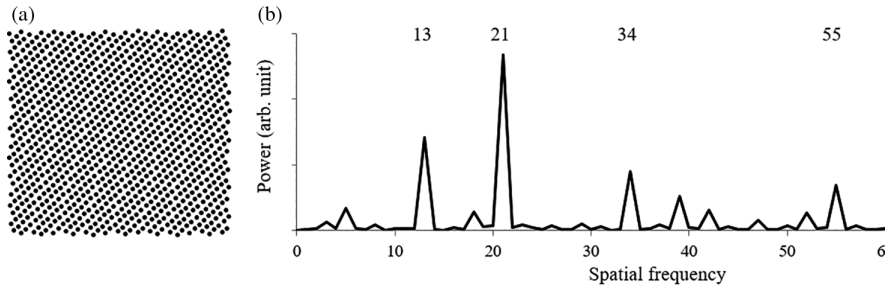

FIGURE 16.18 (a) simulated point pattern of a pineapple model with $n = 1000$, $p = 1$, and $\phi = \phi_\tau$; and (b) Fourier transform result for panel (a).

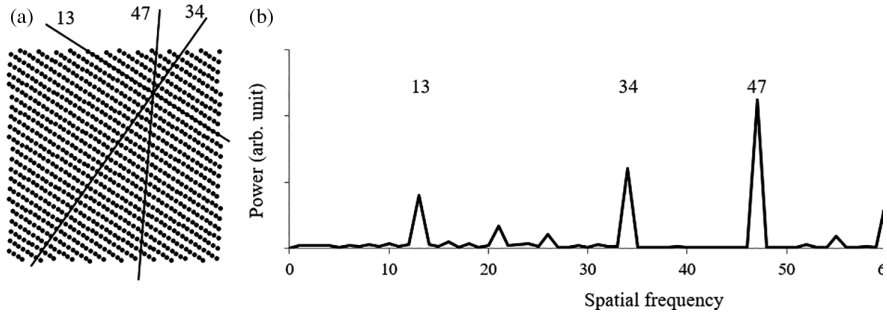

FIGURE 16.19 (a) simulated point pattern of a pineapple model with $n = 1000$, $p = 1$, and $\phi = 137.8°$; and (b) Fourier transform result for panel (a).

When the divergence angles are changed from 137.1° to 137.9° by increments of 0.1°, we recognize some transitions in the parastichy numbers. The transition from $F21$ to $F34$ occur near $\phi = 137.6°$, and $L47$ is observed at divergence angles greater than 137.8°. Here, we recognize some shifts in the parastichy number (Figure 16.20).

The transformation results at 4096 points for $n = 100{,}000$, $p = 1$, and $\phi = \phi_\tau$ (Figure 16.21). Fourier peaks as the spatial frequencies appear at Fibonacci numbers 610, 987, and 1597. Although the magnitude of these powers is different from those in Figure 16.15, they all peak at the same spatial frequency.

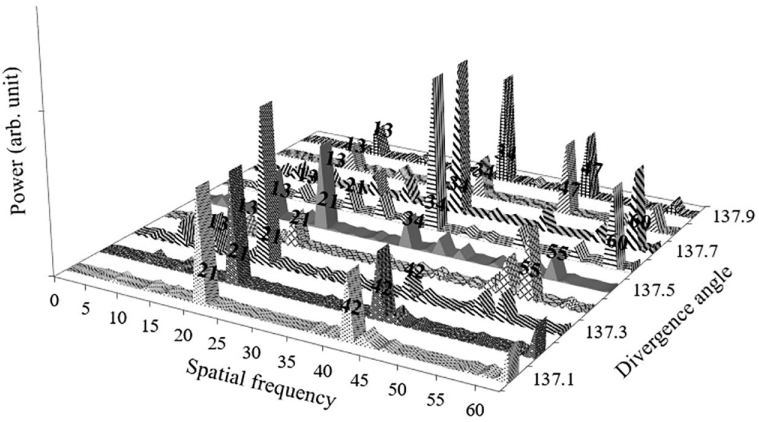

FIGURE 16.20 Fourier transform results for pineapple models with several divergence angles ranging from 137.1° to 137.9°.

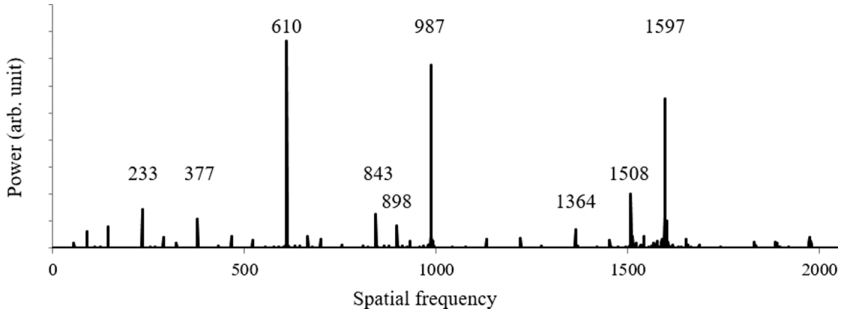

FIGURE 16.21 Fourier transform result for $n = 100000$, $p = 1$, and $\phi = \phi_\tau$.

16.5 DISCUSSION

16.5.1 Difference in the Numbers of Sample Points

This section presents how a different number of sample points affect the Fourier transform results. Figure 16.22a shows the simulated point pattern for a sunflower model with $n = 1000$, $p = 0.5$, $\phi = \phi_\tau$, and 499 sample points. Figure 16.22b shows the Fourier transform result. Fourier peaks at 21, 34, 55, 89, and 144 and are compared with the result with 256 sample points (Figure 16.9); we found that there was a remarkable match between them, except for the power. Note that because the sampling window in the radial direction results in more sample points, more peaks appear.

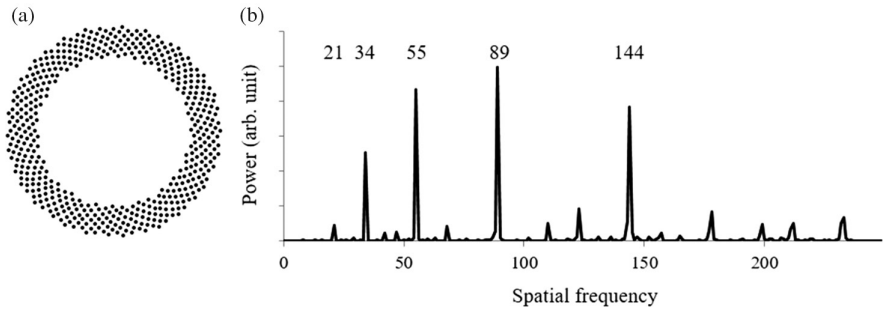

FIGURE 16.22 (a) simulated point pattern for a sunflower model with $n = 1000$, $p = 0.5$, $\phi = \phi_\tau$, and 499 sample points; and (b) Fourier transform result for panel (a).

16.5.2 Difference in Index *p*

This section reports how the parastichy numbers are differed by changing index p using the simulation models. As shown in Figures 16.4 and 16.6, the behavior of the point distribution largely depends on the index p. Figure 16.23a shows the point distribution when $n = 1000$, $p = 1$, and $\phi = \phi_\tau$ in the sunflower model, and Figure 16.23b illustrates the transformation result for 128 points at the outer region. According to the transformation result, the largest Fourier peak is counted as 34, which correspond to the visually counted value.

As for the pineapple model, Figure 16.24a shows the point distribution when $n = 1000$, $p = 2$, and the simulation result shows ununiformity. One hundred twenty-eight points of the upper part of the panel (a) is analyzed by Fourier transform. The parastichy numbers, 13 and 21, are visually confirmed from the distribution image, and they correspond to the transform result.

The results in Figures 16.23 and 16.24 suggest that even with changes in the p values, using the method we propose, we are still able to find parastichy numbers that can correspond to those visually counted.

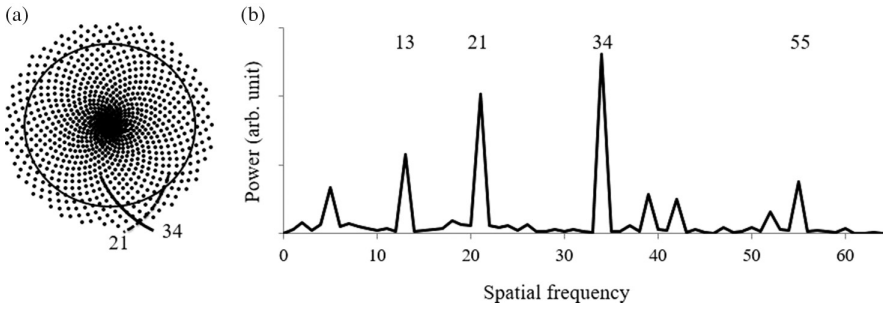

FIGURE 16.23 (a) simulated point pattern for a sunflower model with $n = 1000$, $p = 1$, $\phi = \phi_\tau$, and 128 sample points; and (b) Fourier transform result for panel (a).

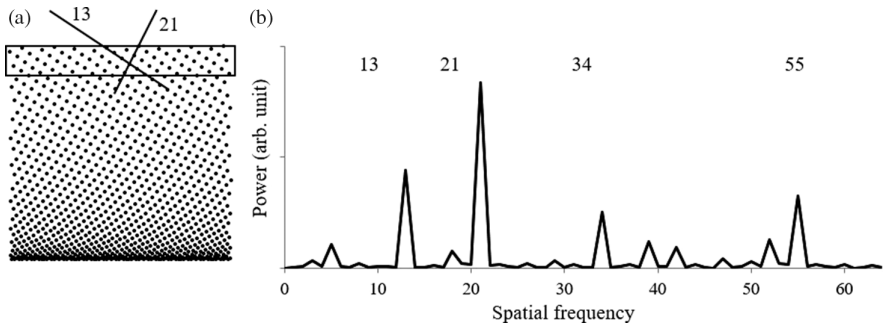

FIGURE 16.24 (a) simulated point pattern for a pineapple model with $n = 1000$, $p = 2$, $\phi = \phi_\tau$, and 128 points in the rectangle; and (b) Fourier transform result for panel (a).

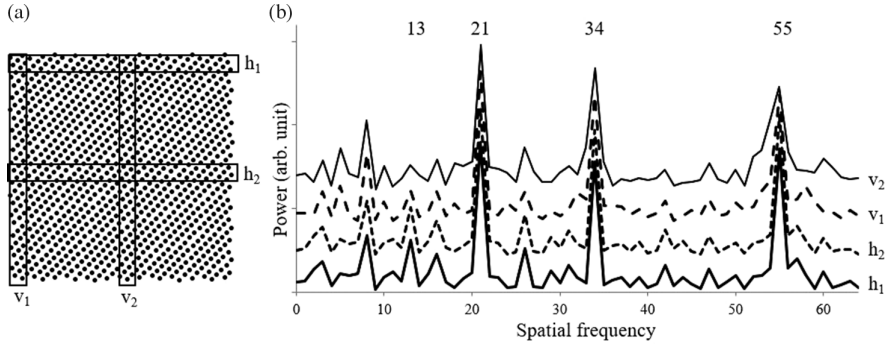

FIGURE 16.25 (a) Fourier transform result by differential sampling area for $n = 1000$, $p = 1$, and $\phi = \phi_\tau$; and (b) Fourier transform result for each area in panel (a).

16.5.3 Sampling Position

This section discusses how the sampling position affects the Fourier transform results. Black rectangles in Figure 16.25a show the sampling area with $n = 1000$, $p = 1$, and $\phi = \phi_\tau$, where h_1 and h_2 are horizontal areas and v_1 and v_2 are vertical areas. Figure 16.25b shows the transform results obtained by sampling in each area. The Fourier peaks, 21, 34, 55, and 89 agree with those visually counted. The Fourier peak 13 for the vertical area (v) is smaller than that of the horizontal area (h). This is because the cycles of the distance interval at the specified place is different between vertical and horizontal regions.

16.6 APPLICATIONS

16.6.1 A Part Sampling

This section presents the effectiveness of a part sampling of an image. In general, a sampling area is assigned as a part of the target image. When 512 points, which is 1/8 of 4096 points in Figure 16.14, are Fourier transformed, the peaks appear at 76, 123, and 199 (Figure 16.26) corresponding to approximately 1/8 of 610, 987, and 1597 in Figure 16.15b, respectively.

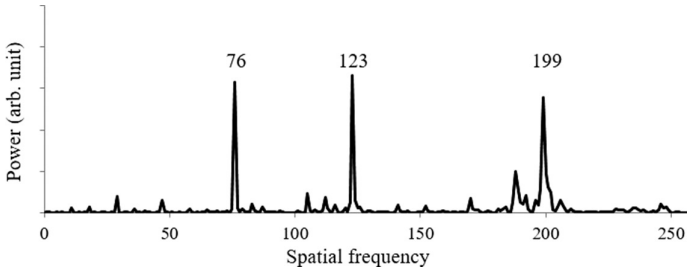

FIGURE 16.26 Fourier transform result for Figure 16.14.

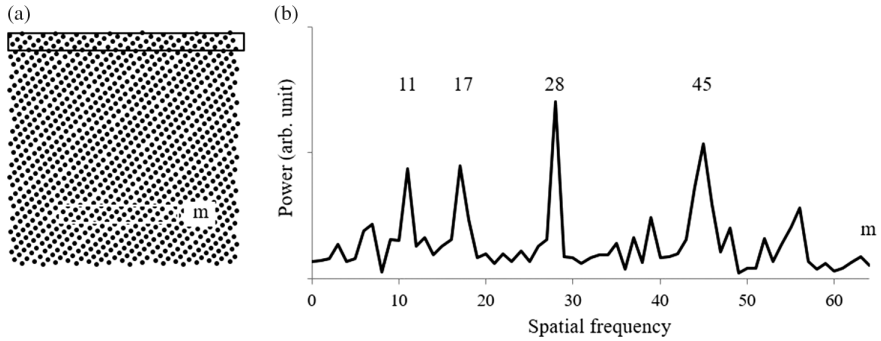

FIGURE 16.27 (a) *m* is a sampling area at 128 points in $n = 1000$, $p = 1.0$, and $\phi = \phi_\tau$; and (b) Fourier transform result for the area *m* in panel (a).

From these results, 199/123 = 1.618 calculated from Figure 16.26 corresponds to 1597/687 = 1.618 in Figure 16.15b. The number value matches up to the third decimal place. This indicates that the proposed method can accurately estimate feature quantities of images even with only a part of target sampling region.

How about planar images? A small rectangle area (*m*) has been sampled from the image in Figure 16.25a as a target area for this study (Figure 16.27). Though the height for the sampled rectangle is the same as the upper rectangle in Figure 16.27, the width is on-half of the upper one. The Fourier peaks appear at 11, 17, 28, and 45 in Figure 16.27b are approximately one-half of the peak values of 21, 34, 55, and 89 in Figure 16.25b. Even with a plane image being analyzed as the sample region, peak values can still be accurately found according to a size of the target region, and that can be treated as the feature quantities of an image.

16.6.2 Evaluation of Disturbance

This section shows the effectiveness of the proposed method in evaluating disturbance. Figure 16.28 shows distribution examples when the divergence angle is nearly the golden angle with $n = 1000$ of the sunflower model. Two hundred fifty-six points are extracted from each figure, and they are analyzed by Fourier transformation using the proposed method. The results are shown in Figure 16.29. The two numbers represent the largest peak and the second largest peak of each image. Because of distribution nonuniformity in (a), disturbance can be easily identified compared to (c) with the golden angle (Figure 16.28). The ratio of the two numbers is also large for (a). On the other hand, even though (b) and (d) appear to be inhomogeneous compared with (c), it is difficult to distinct quantitative differences between (b) and (d). However, Fourier peak patterns of (b) and (d) exhibit a clear difference between them. Therefore, the proposed method is effective to accurately evaluate a disturbance of an image.

A distribution disturbance in the pineapple model is also investigated. Figure 16.30 shows rectangular distributions with the same divergence angle as those in Figure 16.28 when $n = 1000$. Two hundred fifty-six points of the upper part

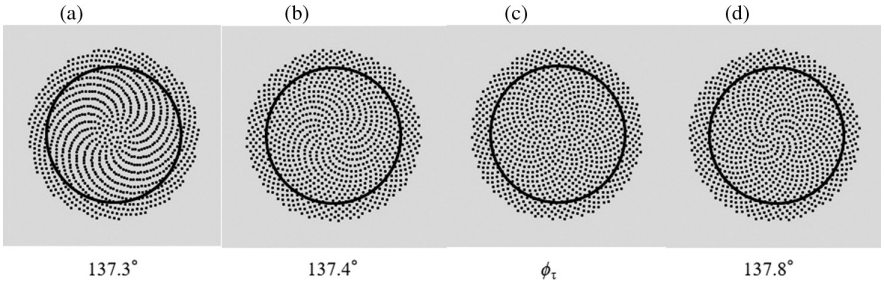

FIGURE 16.28 Differential distribution due to small change in divergence angles under each panel. Sampling areas are outer region of each black circle when the divergence angles are (a) 137.3°, (b) 137.4°, (c) ϕ_τ and (d) 137.8°.

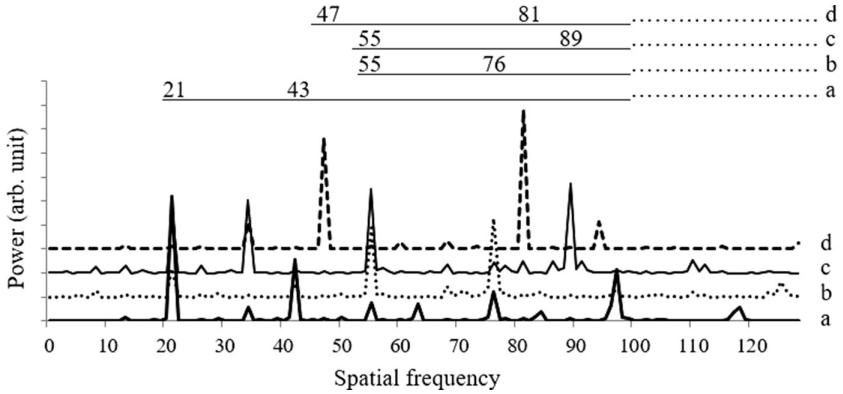

FIGURE 16.29 Fourier transformation results of Figure 16.28.

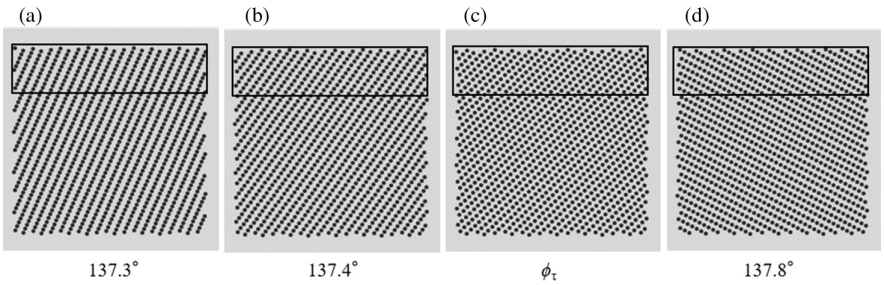

FIGURE 16.30 Differential distribution due to small change in divergence angles under each panel. Sampling areas are upper region of each black rectangle when the divergence angles are (a) 137.3°, (b) 137.4°, (c) ϕ_τ and (d) 137.8°.

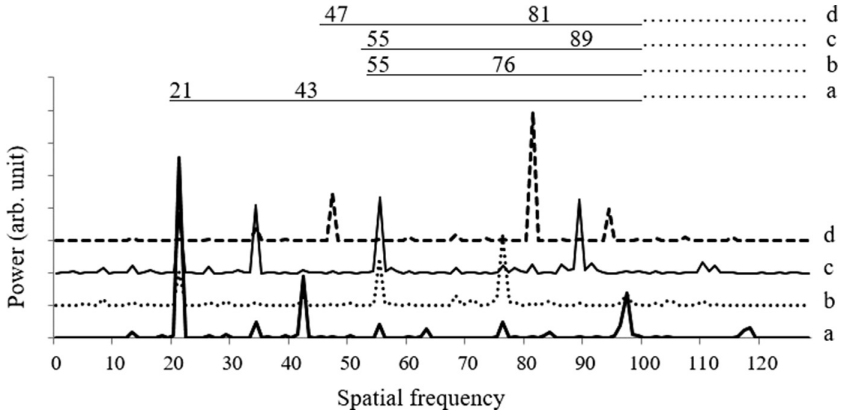

FIGURE 16.31 Fourier transformation results of Figure 16.30.

of each distribution are the sample areas. The transformation results are shown in Figure 16.31. The two numbers are the largest peak and the second largest peak of spatial frequencies of each sample. The two large Fourier peaks are somewhat different magnitude in Figure 16.29, but each position is the same. For (b) and (d), it is, again, difficult to visually identify both figures, yet the numerical values of each spatial frequency clearly differ. Thus, as conclusion, the proposed method is also highly effective to accurately assess a distribution disturbance of a planar image.

16.6.3 Applying to a Real Sunflower

Figure 16.32a is a Russian sunflower with a diameter of 0.3 m. Figure 16.32b shows seed positions extracted from the sunflower. Five hundred twelve points near the

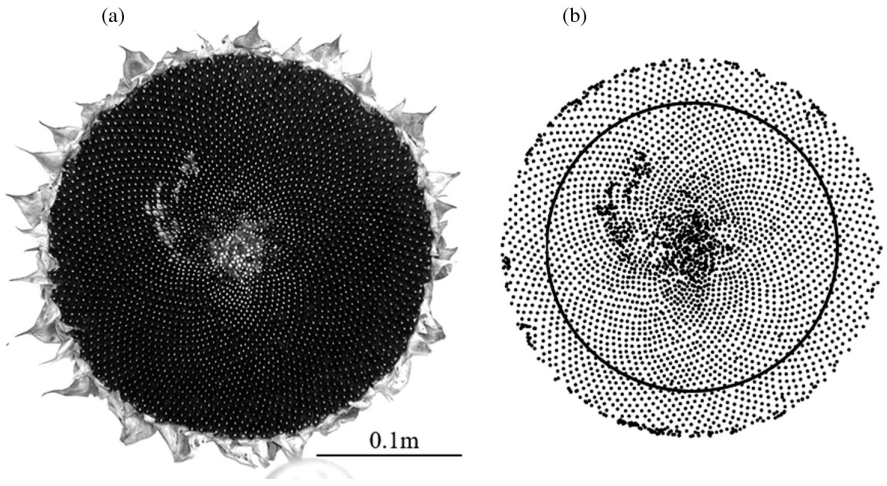

FIGURE 16.32 (a) real Russian sunflower; and (b) reading result of seeds position.

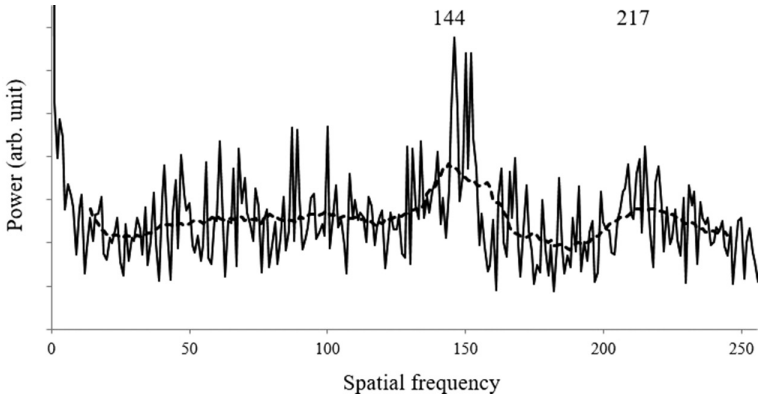

FIGURE 16.33 Transformation result of 512 points near the black circle in Figure 16.32b. Broken line indicates moving averages from the result.

black circle are sampled (Figure 16.32b) and Fourier transformed (Figure 16.33). Many peaks resulted from the transformation indicate many interval cycles of individual living seeds exist (Figure 16.33). The broken line represents the moving averages (Figure 16.33). The ratio, 217/144 = 1.507, of the two peaks is close to the golden ratio. Because the ratio suggests that the seeds are sparsely distributed throughout the head inflorescence, the results demonstrate that the proposed Fourier transform method is useful to evaluate a disturbance of individual seed positions and the distribution tendency of whole seeds.

16.7 SUMMARY

This chapter clearly shows that parastichy numbers for point patterns can be directly measured with the one-dimensional discrete Fourier transforms. The points are patterned from the simulations using the sunflower model and the pineapple model. The detailed pattern analysis using the Fourier method reveals that the parastichy numbers in general cases are a combination of Fibonacci, Lucas, and generalized Fibonacci numbers. In addition, even when the number of measurement points increases to 100,000 points, the parastichy number is still accurately determined by this method.

In the application, even when only a part of the target image is analyzed, the Fourier peaks precisely reflect the image feature quantity. It reveals that the pattern of the adjacent Fourier peaks obtained from the point distribution image is a clear indicator of image disturbance. Moreover, as applying this method to a real sunflower, the feature quantity can also be precisely evaluated.

REFERENCES

Adler, I. 1974. A model of contact pressure in phyllotaxis. *J. Theor. Biol*. 45:1–79.

Adler, I., Barabe, D., and Jean, R. V. 1997. A history of the study of phyllotaxis. *Ann. Bot*. 80:231–244.

Agrawal, A., Kejalakshmy, N., Chen, J., Rahman, B. M. A., and Grattan, K. T. V. 2008. Golden spiral photonic crystal fiber: Polarization and dispersion properties. *Opt. Lett.* 33:2716–2718.

Authier, A. 2001. *Dynamical Theory of X-Ray Diffraction*, 73–78. Oxford University Press.

Douady, S. and Couder, Y. 1992. Phyllotaxis as a physical self-organized growth process. *Phys. Rev. Lett.* 68:2098–2100.

Dunlap, R. A. 1997. *The Golden Ratio and Fibonacci Numbers*, Word Scientific Publishing.

Hofmeister, W. 1868. *Handbuch der PhysiologischenBotanik*, 437–46. Engelmann.

Jean, R. V. 2009. *Phyllotaxis*, Cambridge University Press.

Kikuta, S. 2011. *X-Ray Scattering and Synchrotron Radiation Science-Fundamentals* (*in Japanese*), 144–148, University of Tokyo Press.

Koshy, T. 2001. *Fibonacci and Lucas Numbers with Applications*, 109–115, John Wiley & Sons.

Liew, S. F., Noh, H., Trevino, J., Negro, L. D., and Cao, H. 2011. Localized photonic band edge modes and orbital angular momenta of light in a golden-angle spiral. *Opt. Express.* 19:23631–23642. doi:10.1364/OE.19.023631.

Mathai, A. M. and Davis, T. A. 1974. Constructing the sunflower head. *Math. Biosci.* 20:117–133.

Negishi, R. and Sekiguchi, K. 2007. Pixel-filling by using Fibonacci spiral. *Forma.* 22:207–215.

Negishi, R., Sekiguchi, K., Totsuka, Y., and Uchida, M. 2017. Determining parastichy numbers using discrete Fourier transforms. *Forma.* 32:19–27.

Negro, L. D., Lawrence, N., and Trevino, J. 2012. Analytical light scattering and orbital angular momentum spectra of arbitrary Vogel spirals. *Opt. Express.* 20:18209–18223.

Pennybacker, M. F., Shipman, P. D. and Newell, A. C. 2015. Phyllotaxis: Some progress, but a story far from over. *Physica. D.* 306:48–81.

Swinton, J., Ochu, E., and The MSI Turing's Sunflower Consortium. 2016. Novel Fibonacci and non-Fibonacci structure in the sunflower: Results of a citizen science experiment. *Roy. Soc. Open Sci.* 3:160091.

Trevino, J., Cao, H., and Negro, L. D. 2008. Circularly symmetric light scattering from nanoplasmonic spirals. *Nano Lett.* 11:2008–2016.

Turing, A. M. 1952. Morphogen theory of phyllotaxis, in Saunders, P. T. (Ed.), 1992, *Collected Works of A. M. Turing*: Morphogenesis, North-Holland.

Turing, A. M. 1956. *The Turing Digital Archive*.http://www.turingarchive.org.

Van der Linden, F. M. J. 1990. Creating phyllotaxis, the dislodgement model. *Math. Biosci.* 100:161–199.

Vogel, H. 1979. A better way to construct the sunflower head. *Math. Biosci.* 44:179–189.

Author Query Sheet

Chapter No.: 16

Query No.	Query	Response
AQ 1	Please check if the edited sentence “We will discuss...” is okay.	